Depth-dependent magnetic crossover in a room-temperature skyrmion-hosting multilayer

T. J. Hicken,[1,2] M. N. Wilson,[1,3] Z. Salman,[4] T. Prokscha,[4] A. Suter,[4]
F. L. Pratt,[5] S. L. Zhang,[6] G. van der Laan,[7] T. Hesjedal,[8] and T. Lancaster[1,*]

[1]*Department of Physics, Centre for Materials Physics, Durham University, Durham, DH1 3LE, United Kingdom*
[2]*Department of Physics, Royal Holloway, University of London, Egham, TW20 0EX, United Kingdom*
[3]*Department of Physics and Physical Oceanography, Memorial University of Newfoundland, St. John's, NL A1B 3X7, Canada*
[4]*Paul Scherrer Institute, Forschungsstrasse 111, 5232 Villigen PSI, Switzerland*
[5]*ISIS Pulsed Neutron and Muon Facility, STFC Rutherford Appleton Laboratory, Harwell Oxford, Didcot, OX11 OQX, United Kingdom*
[6]*School of Physical Science and Technology, ShanghaiTech University, Shanghai, 201210, China; ShanghaiTech Laboratory for Topological Physics, ShanghaiTech University, Shanghai 200031, China*
[7]*Diamond Light Source, Harwell Science and Innovation Campus, Didcot, Oxfordshire, OX11 0DE, United Kingdom*
[8]*Department of Physics, Clarendon Laboratory, University of Oxford, Oxford, OX1 3PU, United Kingdom*

(Dated: October 13, 2022)

Skyrmion-hosting multilayer stacks are promising avenues for applications, although little is known about the depth dependence of the magnetism. We address this by reporting the results of circular dichroic resonant elastic x-ray scattering (CD-REXS) and low-energy muon-spin relaxation (LE-μ^+SR) measurements on a stack comprising Ta/[CoFeB/MgO/Ta]$_{16}$ on a Si substrate. Energy-dependent CD-REXS shows a continuous, monotonic evolution of the domain-wall helicity angle with incident energy, consistent with a three-dimensional hybrid domain-wall-like structure that changes from Néel-like near the surface to Bloch-like deeper within the sample. LE-μ^+SR reveals that the magnetic field distribution in the first six layers of the stack is distinct from that in layers further from the surface, quantifying the depth at which the static and dynamic magnetic structure varies. By increasing the applied magnetic field, we find a reduction in the volume occupied by domain walls at all depths, consistent with a crossover into a region dominated by skyrmions above approximately 180 mT.

Several material classes have emerged that host magnetic skyrmion excitations [1, 2], but for applications it is necessary to stabilise skyrmions at room temperature. For this purpose, multilayer systems show promise [3]. These comprise a repeated stack of a magnetic layer and one or more heavy elements, e.g., Ta/CoFeB/MgO. Here, a Dzyaloshinskii-Moriya interaction (DMI) arises from inversion symmetry-breaking at interfaces between the layers, leading to skyrmions that can exist over a wide range of temperature, extending up to 500 K [4]. While skyrmions are often assumed to be a quasi-two-dimensional texture that identically repeats in the third dimension, recent work on Ta/CoFeB/MgO multilayers suggests a variation of the spin texture across multiple repeats of the multilayer [5], with micromagnetic simulations predicting that the helicity of the skyrmion changes from Néel-type at the top surface, to Bloch-type in the middle.

Despite the predictions from micromagnetics being consistent with circular dichroic resonant elastic x-ray scattering (CD-REXS) measurements [6–8] of the system [5, 9–11], a direct measurement of the depth-resolved magnetic environment in the stack has hitherto been lacking. Here we provide these measurements through an investigation of depth-dependent magnetism in the multilayer Ta/[CoFeB/MgO/Ta]$_{16}$ using low-energy muon-spin relaxation (LE-μ^+SR) [12–14]. Previous work [15–18] has shown that bulk μ^+SR [12, 19] is a useful tool in the study of skyrmion systems and their dynamics, while LE-μ^+SR has probed depth-dependent magnetism at interfaces [20] and the behavior of superconducting [21] and magnetic [22] superlattices. However, these studies do not address the evolution of the properties with depth within a repeating structure. Combining our measurements on Ta/[CoFeB/MgO/Ta]$_{16}$ with energy-resolved CD-REXS, we show here how the domain-wall angle and magnetic structure varies with depth, and reveal a crossover in magnetic properties taking place around layer 6 in the stack.

In this system, alternating non-magnetic spacers establish a pronounced dipole-dipole interaction among the CoFeB layers, leading to a unique hybrid three-dimensional (3D) domain wall configuration with a Bloch layer that is located in the middle of the stack [5, 23]. The helicity angle χ, which describes the character of domain walls as well as skyrmions, continuously rotates between the two extremes throughout the stack, with a characteristic profile $\chi(z)$, where z is the depth into the sample. In

this case, the top CoFeB layer favors a Néel-type domain wall with a helicity angle of $\chi = 180°$, while the middle layer that hosts the Bloch point exhibits a Bloch-type domain wall with $\chi = \pm 90°$. The bottom layer is again of Néel-type, but with $\chi = 0°$ [5, 24]. Introducing interfacial DMI moves the Bloch configuration in z [5, 23]. In nonzero external magnetic fields, a similar 3D magnetization characteristic is also expected for skyrmions.

Multilayer Ta/[CoFeB/MgO/Ta]$_{16}$ was grown by magnetron sputtering onto a Si substrate, as described in Refs. [5, 6, 25]. We studied the depth-dependent character of the magnetic domain walls in the multilayer system using CD-REXS [9–11], which is sensitive to the twisting angle of spin spirals and skyrmions, and was previously applied to retrieve the helicity angle χ of a magnetic twisted domain state [10]. Figure 1(a) shows energy-dependent dichroic scattering patterns, obtained on the multilayer sample at room temperature and in zero applied magnetic field. The ring-like magnetic scattering patterns were obtained by integrating several azimuthal angles using the ϕ-axis of the diffractometer. The dichroic patterns feature a dividing vector that separates the blue and red regions of negative and positive dichroic contrast, governed by the dichroism extinction rule [9], as discussed in more detail in Supplementary Section S2 [6]. The azimuthal direction of the dividing vector uniquely reveals the value of χ [10], as shown in Supplementary Fig. S2 [6]. For multilayer systems with a non-uniform $\chi(z)$ profile, the measured χ_m is the average χ from all layers with different weightings. Experimentally, by varying the photon energy across the Fe L_3 edge, or the x-rays incidence angle θ, the weight changes due to the varied sampling depth of the soft x-rays, leading to a different measured average χ_m [11, 24, 26]. For the investigated Ta/[CoFeB/MgO/Ta]$_{16}$ heterostructure, the attenuation length of the x-rays, Λ, is 79 nm at the Fe L_3 edge (707.8 eV) at normal incidence, and 152 nm off-edge (700 eV). The sampling depth varies with the angle between the x-ray beam and surface normal, α, as $\Lambda\cos(\alpha)/2$ [27]. A systematic variation of these parameters therefore provides a strategy for investigating the depth-dependent structural property of a 3D hybrid domain wall.

As can be seen in Fig. 1, the direction of the dividing vector undergoes a gradual change across the photon energy spectrum. Due to the complexity of the multilayered structure, the unambiguous determination of the $\chi(z)$ profile is not as straightforward as for chiral bulk magnets [11, 26]. However, it is possible to obtain qualitative information about the $\chi(z)$ profile. In general, at photon energies far away from the Fe L_3 absorption edge, the soft x-ray attenuation length increases, while it is shorter near the resonance. Consequently, the top part of the multilayer which is closest to the surface contributes more to the total measured χ_m. In other words, if the $\chi(z)$-profile monotonically changes from 180° to 0° as a function of depth, the dividing vector will slightly rotate when changing the photon energy across the Fe L_3 edge. This behavior is consistent with our observations in Fig. 1(a). Furthermore, the sampling depth can be changed over a larger range by varying the incident x-ray angle θ ($\theta = 90° - \alpha$). As shown in Figs. 1(b) and 1(c), by changing θ from 32° to 35°, the CD-REXS pattern reverses sign, suggesting the existence of a smoothly-varying 3D hybrid domain wall structure. Our CD-REXS results are therefore consistent with the micromagnetic simulations of Ta/[CoFeB/MgO/Ta]$_{16}$ [5], suggesting Néel magnetic character near the surface and substrate, and with Bloch-like character in the central region.

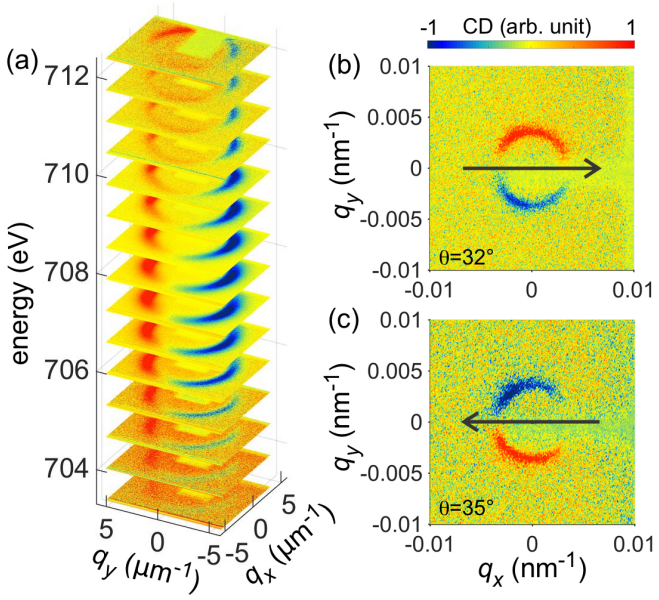

FIG. 1. CD-REXS patterns of the multilayered sample, measured at room temperature in zero magnetic field. (a) Energy-dependent CD-REXS patterns measured at $\theta = 12°$. (b,c) CD-REXS patterns measured at $\theta = 32°$ and 35°, respectively, using a photon energy of 707.8 eV (at the Fe L_3 edge).

Next we turn to the application of LE-μ^+SR to further understand changes in the magnetic states with depth from a local perspective. Simulations of the muon stopping profile in our sample, performed using the TRIM.SP software [6, 28] [Fig. 2(a)] demonstrate how the muons are distributed among the layers at different incident energies E_μ. Owing to the spread in the stopping profile, it is possible to distinguish the top layers from those deeper layers within the sample, although it is not possible to solely probe the layers of the sample nearest the substrate. The profile for a single trilayer is shown in Fig. 2(b) where, for each energy, the multilayer with the most muons stopping in it are compared, normalized by the maximum probability. We find that most muons stop in the Ta layer, with fewest stopping in the MgO layer. There are sufficient muons stopping in all layers to probe

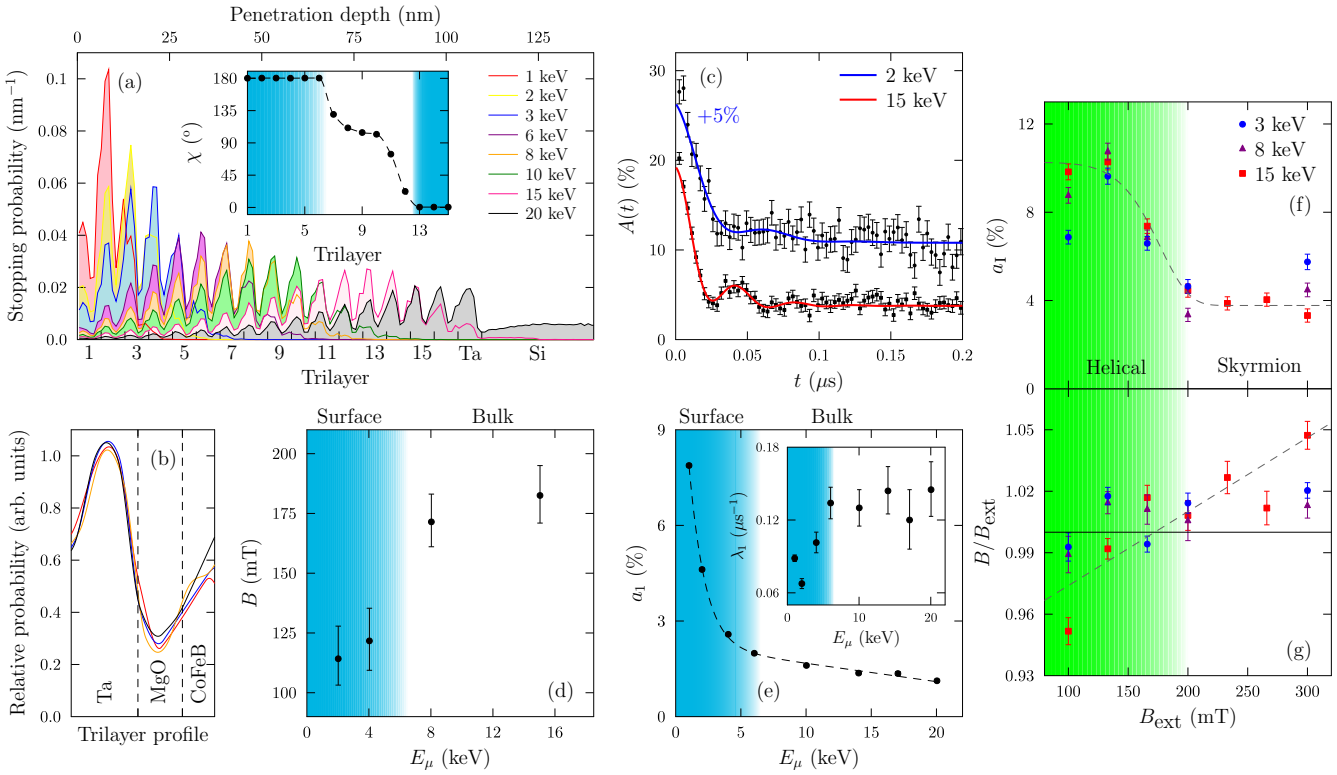

FIG. 2. (a–b) Muon stopping profiles: (a) implantation energy dependence, (b) stopping profile for a single multilayer, showing four energies [colors correspond to (a)]. The inset of (a) shows the results of micromagnetic simulations from Ref. [5]. The helicity angle χ is shown as a function of the layer, showing the evolution from Néel ($\pm180°$ or $0°$, blue shaded regions) to Bloch ($\pm90°$) and back again. (c) Typical ZF μ^+SR spectra $A(t)$ with (d) parameters extracted from fitting. (e) Energy dependence of parameters from fitting TF μ^+SR at 10 mT. (f–g) Field-dependent parameters from fitting TF μ^+SR data, showing (f) the amplitude a_I, and (g) the ratio of B to the applied field B_ext. Dashed lines are guides to the eye.

the magnetism throughout the sample and there is no significant change in the proportion stopping in each material as a function of E_μ.

In zero applied field (ZF) we expect the system to host helical magnetic order. ZF μ^+SR measurements at $T = 295$ K as a function of E_μ show the existence of two distinct regimes of behavior, classified by different implantation depths. (For all measurements the muon spin is initially rotated approximately 10° out of the plane of the film.) The differences with E_μ can be seen in the muon asymmetry $A(t)$, [Fig. 2(c)]. To track the changes we parameterize the data [6, 29–31] using $A(t) = a_1^\mathrm{ZF} \exp(-\lambda_1 t)\cos(\gamma_\mu B t + \phi_0) + a_2^\mathrm{ZF} \exp(-\lambda_2 t) + \sum_{i=3}^{4} a_i \exp\left(-\sigma_i^2 t^2\right)$. Many of these parameters are energy-independent [6], leaving the component with amplitude a_1^ZF containing the majority of the information about the variation of the magnetic properties with depth. The a_1^ZF component arises from muons that stop in sites where the muon spin and local field B are not parallel, leading to coherent spin precession. The relaxation rate of this component depends both on the static distribution of fields at the muon site, and the dynamic fluctuations. The change in B with E_μ is shown in Fig. 2(d).

There are two regimes evident in Fig. 2(d), with the measurements at 4 keV and below showing different behavior to those at 8 keV and above. Comparing with Fig. 2(a), we suggest a surface regime is formed from approximately the first 5–6 stacks nearest the surface, corresponding to a penetration depth up to $\simeq 25$ nm. At higher implantation energy, the local field at the muon sites increases sharply in magnitude, suggesting a different magnetic structure to that found near the surface. The approximately-constant value of the relaxation rates implies the relaxation is dominated by dynamic effects (since if it were dominated by the static magnetism, we expect $\lambda \propto B^2$), suggesting no significant change in dynamics with depth on the muon timescale. These measurements therefore suggest a change to the static magnetic structure beyond around layer 6 of the sample, such that the average local field at the muon sites increases. In micromagnetic simulations [5] a change from Néel-type skyrmions at the surface to Bloch-type below layer 6 is observed, as reproduced in the inset of Fig.2(a). The increase of field away from the surface observed with LE-μ^+SR is consistent with changes in the magnetism suggested by micromagnetic simulations and observed with

CD-REXS, giving quantitative agreement between the expected depth of these changes.

To explore these changes further, TF μ^+SR measurements were performed at 295 K as a function of E_μ in an applied magnetic field of 10 mT, applied perpendicular to the film, for which we expect the system to remain helically magnetically ordered. For these data we fit the number of counts in each detector simultaneously, using the polarization $P_x(t) = \sum_{i=1}^{2} a_i \exp(-\lambda_i t)\cos(\gamma_\mu B t + \phi_0)$, where, due to the difficulty resolving two different fields at the muon site (in particular due to the large λ_2), we constrain the fits to share B between the two components. We find many parameters to be energy-independent [6]. The energy-dependent parameters, a_1 and λ_1, are shown in Fig. 2(e).

We interpret the two different components as arising from muons stopping at different sites in the sample. Since there is little change in the proportion of muons stopping in each material within a trilayer as a function of energy [Fig. 2(b)], the results likely reflect changes in the magnetism as a function of depth, similar to that reported above for ZF measurements. The site contributing to the a_1 component experiences a small internal field and has a small relaxation rate, leading to coherent precession in the applied magnetic field. This suggests these sites constitute regions of disordered magnetic field, such as domain wall-like regions. This relaxation rate increases with depth, suggesting the frequency of dynamic fluctuations decreases at these sites. This might be expected as surface-dominated states have dynamics arising from rapid fluctuations on a relatively-short lengthscale (as the system tries to find a configuration that satisfies the constraint of the surface) to one where longer wavelength collective excitations dominate in the bulk of the material. As E_μ increases, the amplitude decreases, consistent with fewer surface-state muon-sites being realized with depth. We again see a crossover around layer 6 of the material. Although this appears relatively smooth in Fig. 2(e), this at least partially reflects the fact that the stopping profile is spread across several layers at each implantation energy. The changes observed in the TF measurements coincide with the change in magnetic structure seen from the ZF results, implying that the same crossover with depth is responsible for both measurements. We therefore have a picture of (i) a static magnetic structure changing with depth (from those muon sites in large local magnetic field giving rise to the ZF signal), and (ii) the number of domain wall sites decreasing with depth, whilst the dynamics on the muon-timescale in these sites also decreases (from muon sites in regions with small local field). For both types of muon site, the environment changes rapidly around layer 6.

To access the region of the phase diagram where skyrmions are stabilized, further TF μ^+SR measurements were performed as a function of larger magnetic fields, at $T = 295$ K using implantation energies: 3, 8, and 15 keV. For these data $P_x(t) = a_\mathrm{I}\exp(-\lambda_\mathrm{I} t)\cos(\gamma_\mu B t + \phi_\mathrm{B}) + a_\mathrm{II}\exp\left(-\sigma_\mathrm{II}^2 t^2\right)$ is found to describe the behavior over the entire dataset. Most parameters are found to be independent of applied magnetic field or arising from background effects [6], hence we focus on the component with amplitude a_I, arising from muons stopping in sites where the spin precess in a local field B, which is found to be close to the applied field. This implies we are again sensitive to the domain-wall sites where the local field is small in these measurements. The field-dependent changes in a_I and B are shown in Fig. 2(f–g).

The proportion of muons stopping in the sample and giving coherent spin precession decreases as B_ext is increased [Fig. 2(f)]. This effect is approximately twice the size of that observed as a function of implantation energy in the low-TF measurements, showing that field leads to a more rapid decrease in the occurrence of these domain-wall environments compared to their variation with depth. This picture is supported by the results of x-ray ptychography measurements [5] that suggest just such a change in magnetic structure with out-of-plane magnetic field, such that skyrmions become the dominant magnetic defect above ∼150 mT. The skyrmions represent a limiting case of the domain-wall structure, minimising the sample volume occupied by the low-field muon stopping sites. This is consistent with our measurement in which, around 180 mT, the amplitude parameter ceases changing, suggesting a crossover to a different regime. We therefore suggest that this crossover can be seen at all implantation energies, and that the plateau of a_I indicates the stabilization of skyrmions at each depth within the stack that we have probed.

There appears to be a weak dependence of the ratio B/B_ext with B_ext, Fig. 2(g). As B_ext increases, the enhancement of B becomes larger, from predominantly below the applied field, to above, most pronounced at 15 keV. The crossover between these regions appears to approximately coincide with the transition to skyrmion-dominated magnetic structures. Further, the reduction in a_I in the skyrmion-stabilized phase might suggest the contribution of muons in sites where the spin is relaxed too rapidly to be detected, reducing a_I, consistent with the response seen in other skyrmion systems [16–18], where in these bulk materials the relaxation is strongly enhanced at the center of the skyrmion lattice phase, even when the skyrmion lattice is not the majority phase.

In summary, our LE-μ^+SR and CD-REXS measurements identify changes in the magnetism of the Ta/[CoFeB/MgO/Ta]$_{16}$ multilayer stack on a Si substrate as a function of both depth and applied field. CD-REXS demonstrates the continuous evolution of the helicity angle with depth, while ZF μ^+SR shows that the magnetism in the top six layers of the multilayer stack have a different static and dynamic magnetic structure to those further from the surface. The layer at

which this crossover is observed provides quantitative agreement with predictions from simulations [5, 24]. We also identify a decrease in the volume occupied by domain walls with both depth and applied magnetic field, with the latter undergoing a crossover to a regime dominated by skyrmions around 180 mT. Our work highlights the utility of the LE-μ^+SR technique in studying multilayer skyrmion systems, providing unique insights into the depth dependence of the magnetic textures and their properties. These findings confirm results from computational predictions, and paves the way for future investigations to experimentally verify a number of other computational works on technological applications of skyrmion-hosting systems. Determining the depth-dependence of the magnetic properties of multilayered systems is of paramount importance for their incorporation in device applications.

Part of this work was carried out at the Paul Scherrer Institut, Switzerland; we are grateful for the provision of beamtime. The authors acknowledge Diamond Light Source for beamtime on beamline I10 under proposal SI-18898. The project was funded by EPSRC (UK) (Grant No: EP/N032128/1). M.N. Wilson acknowledges the support of the Natural Sciences and Engineering Research Council of Canada (NSERC). Research data from this paper will be made available via Durham Collections at XXX. For the purpose of open access, the authors have applied a Creative Commons Attribution (CC BY) licence to any Author Accepted Manuscript version arising.

[1] T. Lancaster, Contemp. Phys. **60**, 246 (2019).
[2] N. Nagaosa and Y. Tokura, Nature Nanotechnol. **8**, 899 (2013).
[3] W. Jiang, G. Chen, K. Liu, J. Zang, S. G. E. Te Velthuis, and A. Hoffmann, Phys. Rep. **704**, 1 (2017).
[4] S. Zhang, J. Zhang, Y. Wen, E. M. Chudnovsky, and X. Zhang, Appl. Phys. Lett. **113**, 192403 (2018).
[5] W. Li, I. Bykova, S. Zhang, G. Yu, R. Tomasello, M. Carpentieri, Y. Liu, Y. Guang, J. Gräfe, M. Weigand, D. M. Burn, G. van der Laan, T. Hesjedal, Z. Yan, J. Feng, C. Wan, J. Wei, X. Wang, X. Zhang, H. Xu, C. Guo, H. Wei, G. Finocchio, X. Han, and G. Schütz, Adv. Mater. **31**, 1807683 (2019).
[6] See supplemental material for sample preparation details, information on the different experimental techniques, and more detailed information of the fitting of experimental data that would allow one to recreate our analysis.
[7] G. van der Laan, C. R. Physique **9**, 570 (2008).
[8] S. L. Zhang, G. van der Laan, and T. Hesjedal, Nat. Commun. **8**, 14619 (2017).
[9] S. L. Zhang, G. van der Laan, and T. Hesjedal, Phys. Rev. B **96**, 094401 (2017).
[10] S. Zhang, G. van der Laan, W. Wang, A. Haghighirad, and T. Hesjedal, Phys. Rev. Lett. **120**, 227202 (2018).
[11] S. Zhang, G. van der Laan, J. Müller, L. Heinen, M. Garst, A. Bauer, H. Berger, C. Pfleiderer, and T. Hesjedal, Proc. Natl. Acad. Sci. U.S.A. **115**, 6386 (2018).
[12] S. J. Blundell, R. De Renzi, T. Lancaster, and F. L. Pratt, *Muon Spectroscopy: An Introduction* (Oxford University Press, Oxford, 2022).
[13] T. Prokscha, E. Morenzoni, K. Deiters, F. Foroughi, D. George, R. Kobler, A. Suter, and V. Vrankovic, Nucl. Instrum. Meth. A **595**, 317 (2008).
[14] E. Morenzoni, H. Glückler, T. Prokscha, H. P. Weber, E. M. Forgan, T. J. Jackson, H. Luetkens, C. Niedermayer, M. Pleines, M. Birke, A. Hofer, J. Litterst, T. Riseman, and G. Schatz, Physica B: Cond. Matter **289**, 653 (2000).
[15] T. Lancaster, R. C. Williams, I. O. Thomas, F. Xiao, F. L. Pratt, S. J. Blundell, J. C. Loudon, T. Hesjedal, S. J. Clark, P. D. Hatton, M. Ciomaga Hatnean, D. S. Keeble, and G. Balakrishnan, Phys. Rev. B **91**, 224408 (2015).
[16] K. J. A. Franke, B. M. Huddart, T. J. Hicken, F. Xiao, S. J. Blundell, F. L. Pratt, M. Crisanti, J. A. T. Barker, S. J. Clark, A. Štefančič, M. Ciomaga Hatnean, G. Balakrishnan, and T. Lancaster, Phys. Rev. B **98**, 054428 (2018).
[17] T. J. Hicken, S. J. R. Holt, K. J. A. Franke, Z. Hawkhead, A. Štefančič, M. N. Wilson, M. Gomilšek, B. M. Huddart, S. J. Clark, M. R. Lees, F. L. Pratt, S. J. Blundell, G. Balakrishnan, and T. Lancaster, Phys. Rev. Res. **2**, 032001(R) (2020).
[18] T. J. Hicken, M. N. Wilson, K. J. A. Franke, B. M. Huddart, Z. Hawkhead, M. Gomilšek, S. J. Clark, F. L. Pratt, A. Štefančič, A. E. Hall, M. Ciomega Hatnean, G. Balakrishnan, and T. Lancaster, Phys. Rev. B **103**, 024428 (2021).
[19] S. J. Blundell, Contemp. Phys. **40**, 175 (1999).
[20] J. A. Krieger, Y. Ou, M. Caputo, A. Chikina, M. Döbeli, M.-A. Husanu, I. Keren, T. Prokscha, A. Suter, C.-Z. Chang, J. S. Moodera, V. N. Strocov, and Z. Salman, Phys. Rev. B **99**, 064423 (2019).
[21] A. Suter, E. Morenzoni, T. Prokscha, B. M. Wojek, H. Luetkens, G. Nieuwenhuys, A. Gozar, G. Logvenov, and I. Božović, Phys. Rev. Lett. **106**, 237003 (2011).
[22] A. V. Boris, Y. Matiks, E. Benckiser, A. Frano, P. Popovich, V. Hinkov, P. Wochner, M. Castro-Colin, E. Detemple, V. K. Malik, C. Bernhard, T. Prokscha, A. Suter, Z. Salman, E. Morenzoni, G. Cristiani, H.-U. Habermeier, and B. Keimer, Science **332**, 937 (2011).
[23] W. Legrand, J.-Y. Chauleau, D. Maccariello, N. Reyren, S. Collin, K. Bouzehouane, N. Jaouen, V. Cros, and A. Fert, Sci. Adv. **4**, eaat0415 (2018).
[24] Y. Guang, K. Ran, J. Zhang, Y. Liu, S. Zhang, X. Qiu, Y. Peng, X. Zhang, M. Weigand, J. Gräfe, G. Schütz, G. van der Laan, T. Hesjedal, S. Zhang, G. Yu, and X. Han, Phys. Rev. Lett. **127**, 217201 (2021).
[25] D. M. Burn, S. L. Zhang, G. Q. Yu, Y. Guang, H. J. Chen, X. P. Qiu, G. van der Laan, and T. Hesjedal, Phys. Rev. Lett. **125**, 137201 (2020).
[26] K. Ran, Y. Liu, H. Jin, Y. Shangguan, Y. Guang, J. Wen, G. Yu, G. van der Laan, T. Hesjedal, and S. Zhang, Nano Lett. **22**, 3737 (2022).
[27] G. van der Laan, S. L. Zhang, and T. Hesjedal, AIP Adv. **11**, 015108 (2021).
[28] E. Morenzoni, H. Glückler, T. Prokscha, R. Khasanov, H. Luetkens, M. Birke, E. Forgan, C. Niedermayer, and

M. Pleines, Nucl. Instrum. Meth. B **192**, 254 (2002).
[29] F. L. Pratt, Physica B: Conden. Matter **289**, 710 (2000).
[30] F. James and M. Roos, Comp. Phys. Comm. **10**, 343 (1975).
[31] A. Suter and B. Wojek, Phys. Procedia **30**, 69 (2012)